Shishir Chaudhary*, M. Sankar, V.V. Satya Prasad, R.G. Baligidad and A.A. Gokhale

Effect of tungsten and zirconium on structure and properties of niobium

https://doi.org/10.1515/htmp-2016-0227
Received October 31, 2016; accepted December 9, 2017

Abstract: The individual and combined effects of W and Zr additions on macrostructure, microstructure and mechanical properties of Nb have been investigated. Nb, Nb-10 wt% W, Nb-2.5 wt% Zr and Nb-10 wt% W-2.5 wt% Zr alloy ingots were prepared by electron beam drip melting using high purity Nb, W and Zr rods. Additions of W and Zr resulted in significant improvement in hardness and room temperature tensile strength. It is seen that the effect of 10 wt% W addition is more than that of 2.5 wt% Zr addition in improving room temperature strength of Nb, although on 'per wt% addition' basis, Zr is a more effective strengthener than W. It is also observed that the cumulative effects of 10 wt% W and 2.5 wt% Zr on grain refinement and strengthening are more than their respective individual effects.

Keywords: EB drip melting, Nb-based alloys, macro- and microstructure, mechanical properties

Introduction

Future aerospace applications such as advanced turbojet and scramjet engines used in subsonic, supersonic and hypersonic flights will require materials with ever increasing temperature- and load-bearing capabilities for improved performance under extreme environmental conditions. The current state-of-the-art super-alloys can be utilized to a maximum temperature of 1070–1100°C, and the need for viable materials with greater than 1100°C temperature capabilities has long been felt, and work is being pursued in different directions to develop materials with very high temperature capability [1, 2].

One such area is the development of ceramics and composite materials, which have very good high temperature capability. However, designers frequently find that these materials cannot be easily fabricated into the shapes required. In other instances, users of high temperature materials are rediscovering that the applicability of advanced non-metallic and composite materials may be limited by their relatively low thermal conductivity. Alloys with good thermal conductivity require less intense cooling in applications such as turbine hot sections.

Niobium is one of the most promising refractory metals for ultra-high temperature structural applications, because of its very high melting temperature. It is the lightest refractory metal, with density close to that of nickel, and with good thermal conductivity (65.3 W/mK at 600°C) and low ductile-brittle transition temperature. Its bcc structure enables a higher solubility of alloying elements. It has excellent formability and weldability and is not susceptible to low temperature notch sensitivity. However, although niobium is attractive in terms of high melting temperatures and good room temperature ductility, its applications have been limited because of its poor high temperature strength and oxidation resistance. The strength of niobium decreases above 930°C. Niobium is easily oxidized at about 250°C, more rapidly so at temperatures above 500°C. Its high temperature oxidation resistance and high temperature strength need to be improved for long-term very high temperature structural applications [2]. Nevertheless, it is noteworthy that this metal possesses qualities that cannot be offered by any other type of material. Hence, considerable effort has been made to compensate for its disadvantages by engineering design of the components.

An excellent review paper published by Wilcox [3] provides various strengthening mechanisms applicable to Niobium (Nb). Nb can be strengthened by (a) cold working, (b) solid solution strengthening, (c) second-phase particle hardening and (d) composite strengthening by additions of strong fibres in high volume fractions. Solid solution strengthening and dispersion strengthening are the predominant mechanisms used for increasing the elevated temperature strength of Nb. Alloying elements such as Mo and W, which are group VIA elements and which go into solid solution with Nb, are the most effective in imparting high temperature strength.

***Corresponding author: Shishir Chaudhary,** Defence Metallurgical Research Laboratory, Kanchanbagh, Hyderabad, 500058, India, E-mail: ishishirchaudhary@gmail.com
M. Sankar, V.V. Satya Prasad, R.G. Baligidad, Defence Metallurgical Research Laboratory, Kanchanbagh, Hyderabad, 500058, India
A.A. Gokhale, Department of Mechanical Engineering, Indian Institute of Technology Bombay, Powai, Mumbai, 400076, India

However, when added in sufficient quantity to give appreciable strengthening effect, these elements adversely affect the workability, formability and weldability. More recently, work on equiatomic high entropy alloy Nb-Mo-Cr-Ti-Al showed room temperature strength to be about 1 GPa with good retention of strength and ductility up to 800°C [4]. Another potent strengthening mechanism characteristic of most of the high strength alloys is the interaction between one of the reactive elements Zr or Hf and C, O or N to form fine dispersoids. The dispersoids are very effective with respect to high temperature strengthening. However, recent work based on first principles shows that interstitials are harmful from hardness as well as ductility point of view, while minor additions of Si increase hardness as well as ductility [5].

In searching for ways to increase high-temperature strength, significant activities in Nb alloy development were undertaken during the 1950s, 1960s and early 1970s. Several potential alloys were developed [6, 7]. The most common high-temperature niobium alloys are Nb–1 Zr, C-103 (Nb–10 Hf–1 Ti), Cb-752 (Nb–10 W–2.5 Zr) and C-129 y (Nb–10 W–1 Hf–0.1 Zr) [8–10]. These alloys were extensively explored as candidate materials for nuclear applications and structural components in aircraft, space vehicles, rockets, etc. In addition to the space and nuclear applications, Nb-based alloys are being used for electronic, high energy physics and chemical process industries.

In spite of many component development studies reported above, systematic studies on the effect of single and multiple alloying additions on microstructure and mechanical properties of niobium are scanty in the literature. The objective of the present work is to study the individual as well as combined effect of 10 wt% W and 2.5 wt% Zr on macro- and micro structure, and mechanical properties of as cast electron beam (EB) melted Cb–752 alloy ingots.

Experimental procedure

Conventional melting and casting techniques are unsuitable for the production of Nb and Nb-based alloys since the melting temperatures of these metals are above the working temperatures of common refractories. Electron beam drip melting (EBM) process is widely used for melting niobium and its alloys. EBM process is distinguished by its superior refining capacity and a high degree of flexibility of heat source. This process combines the possibilities of melting metals in a very high vacuum as well as heating to a very high temperature. These characteristics make this melting technique suitable for the melting of Nb-based alloys [11, 12]

In the present work, the consumable electrodes for EBM have been prepared by TIG welding of high purity W and Zr rods to high purity Nb rods under argon atmosphere. The electrodes conformed to Nb–9 wt% W, Nb–4.7 wt% Zr and Nb–9.5 wt% W–4.23 wt% Zr composition. The relative weights of Nb, W and Zr have been calculated keeping the evaporation losses of Nb and Zr in view during EBM [13, 14]. The typical TIG welded Nb–9.5 wt% W–4.23 wt% Zr electrodes are shown in Figure 1.

Figure 1: Typical TIG welded Nb–9.95 wt% W–4.23 wt% Zr electrodes.

The pure Nb, Nb–9 wt% W, Nb–4.7 wt% Zr and Nb–9.5 wt% W–4.23 wt% Zr electrodes were EB drip melted. EB drip melting was carried out at a melt rate of 5 kg/h and a power input of 45 kW, and cast in 60 mm dia. water cooled copper crucible to produce 60 mm diameter and 150 mm long ingots. The EB drip melting process parameters are listed in Table 1. The schematic diagram of EBM of TIG welded electrode is shown in Figure 2. The EB melting process was carried out in manual mode by alternately focusing the EB between the consumable electrode to melt the tip and the surface of the melt pool in the crucible.

These ingots were homogenized at 1400 °C for 4 h under 10^{-4} mbar vacuum. The chemical composition of the ingots was determined as follows. W and Zr were analysed by inductively coupled plasma optical emission

Table 1: EB drip melting process parameters.

Electrode composition (wt%)	Electrode dia. (mm)	EB ingot dia. (mm)	EB power kW	Vacuum level in melt chamber mbar	Melt rate kg/h
Nb	30	60	40–45	1×10^{-3} to 1×10^{-4}	5
Nb–9 W	30	60	40–45	1×10^{-3} to 1×10^{-4}	5
Nb–4.7 Zr	30	60	40–45	1×10^{-3} to 1×10^{-4}	5
Nb–9.5 W–4.23 Zr	30	60	40–45	1×10^{-3} to 1×10^{-4}	5

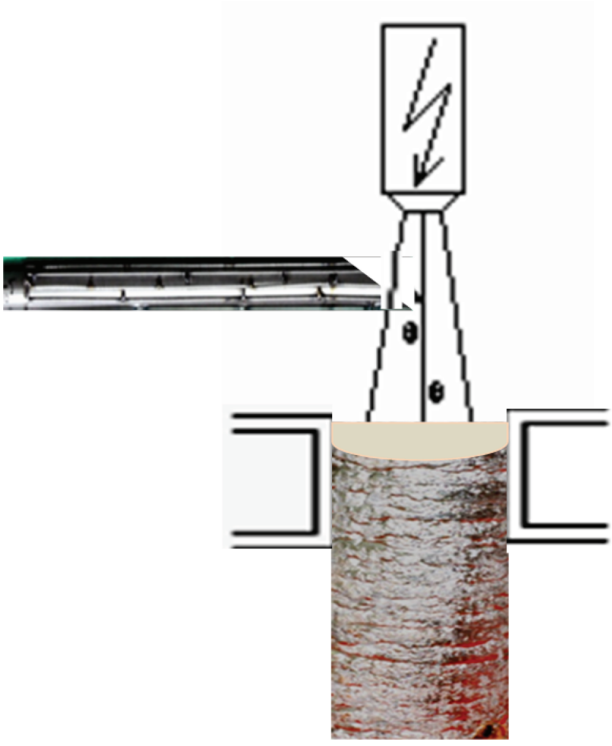

Figure 2: Schematic diagram of electron beam drip melting.

spectroscopy method (ICPOES). LECO carbon and sulphur analyser were used for carbon analysis, whereas hydrogen determinator was used for hydrogen analysis. The analysis of oxygen and nitrogen was carried out using LECO Oxygen – Nitrogen Gas Analyser.

Longitudinal sections of 5 mm and 10 mm thickness were cut from the EBM ingots using band saw. Cutoff sections of 10 mm thickness were mechanically polished with 60–600 grit SiC abrasive papers and etched with an etchant comprising of three parts HF + two parts HNO_3 + 4 parts H_2O by volume for examination of macrostructure. Cutoff sections of 5 mm thickness from cast alloy were mechanically polished with 60–1200 grit SiC abrasive papers followed by 1 µm grade diamond powder polishing to ensure complete removal of scratches. The polished samples were then etched using an etchant comprising of a mixture of 30 ml HF, 15 ml HNO3, 15 ml HCl and 10 ml water by volume for microstructural examination by optical microscope. The phases present in the alloys were also identified by Philips X-ray diffractometer with monochromatic CuKα (λ = 1.540562 Å) radiation. The crystal structure of individual phases was identified by matching the characteristic X-ray diffraction (XRD) peaks against JCPDS data. Lattice parameters were also determined using JCPDS data.

Tensile samples were examined for their internal soundness using X-ray radiography before testing. Bulk hardness measurements were made on the metallography samples using a Leco LV700 Vickers hardness testing machine using a load of 30 kgf. Tensile specimens of 4.0 mm gauge diameter and 20-mm gauge length were prepared in the longitudinal direction of the cast ingots conforming to ASTM E8M standard. Tensile tests were carried out at room temperature in an Instron Universal testing machine at an initial strain rate of 0.8×10^{-4} per second. The fracture surfaces of tensile tested samples were examined under a Leo 440i scanning electron microscope (SEM).

Results and discussion

The surfaces of the EB melted Nb ingots exhibited ripples and folds typical of semi-continuous casting processes (Figure 3). The concentration of W and Zr in TIG welded electrodes (based on weighted averages on quantities of individual metals) and EB drip melted ingots are shown in Tables 1 and 2 respectively. The concentrations of W and Zr in TIG welded electrodes were selected based on our earlier experience on the losses of Nb (about 8 to 10 %) and Zr (40 to 50 %), and that W undergoes negligible losses during EB melting [12–14]. Thus, the starting concentration of W in the welded electrodes was taken to be less (9 and 9.5 wt%) than the proposed content of 10 wt% W in the alloy, while the concentration of Zr was taken to be more (4.7 and 4.23 wt%) than the proposed alloy concentration of 2.5 wt% Zr. As expected, the concentrations of Zr and W

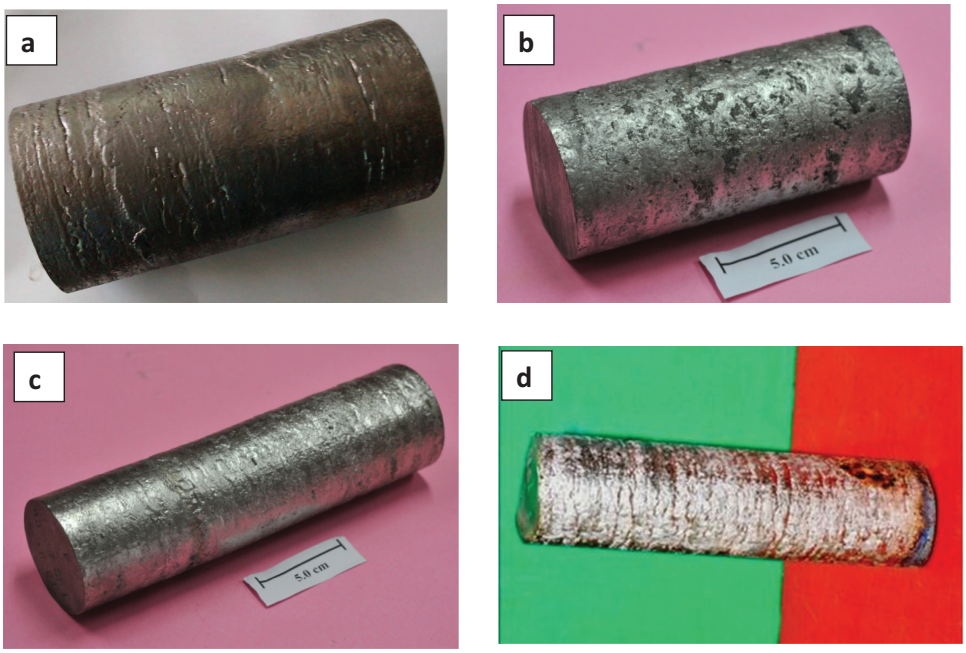

Figure 3: 60 mm diameter EB drip melted (a) Nb, (b) Nb–10 W, (c) Nb–2.5 Zr and (d) Nb–10 W–2.5 Zr ingots.

Table 2: Chemical analysis of EB drip melted ingots.

Alloy	Alloy nominal composition (wt%)	Alloy actual composition (wt%)					
		W	Zr	C	N	O	H
	Nb	–	–	0.003	0.005	0.005	0.0004
Alloy 1	Nb–10 W Alloy	9.98	–	0.003	0.007	0.005	0.0003
Alloy 2	Nb–2.5 Zr	–	2.7	0.005	0.006	0.006	0.0004
Alloy 3	Nb–10 W–2.5 Zr	10.7	2.5	0.003	0.009	0.007	0.0006

in the EB melted Nb ingots are close to the nominal values (Table 2). The concentrations of interstitial impurities (C, N, O and H) in Nb and other three alloys are very low and of the same levels (Table 2). The reasons for the unequal losses of various elements during EB melting are explained as follows. The vacuum level maintained in the EB melt chamber was of the order of 10^{-3}–10^{-4} mbar. Since the vapour pressure of Nb is 10^{-3} mbar, which is close to the vacuum level in the melt chamber, its evaporation losses are of moderate level. However, the vapour pressure of Zr is much higher (10^{-1} mbar) resulting in appreciable evaporation loss of Zr during EB melting. The vapour pressure of W is much lower (10^{-5} mbar) than the chamber pressure and hence the loss of W is negligible. The vapour pressures of Nb, W and Zr stated above are corresponding to the operating temperature of EB melting based on literature (~2750°C).

Macrostructures of the longitudinal section of all the alloy ingots show columnar grains aligned almost parallel to the ingot axis demonstrating that the solidification was directional (Figure 4). During EBM there is uniform distribution of heat across the metal bath due to scanning of EB across the entire surface of liquid metal. The cooling of the liquid metal pool takes place mainly by extraction of the heat from the bottom of the ingot. These factors contribute to high thermal gradients and directional solidification. No solidification substructure could be seen at the optical level. Alloy 1 (Nb–10 W), Alloy 2 (Nb–2.5 Zr) and Alloy 3 (Nb–10 W–2.5 Zr) exhibit much finer solidification structure as compared to EB melted pure Nb. All the three alloys exhibited a single-phase microstructure at optical level (Figure 5). The individual additions of 10 wt% W and 2.5 wt% Zr have resulted in significant reduction in grain size of Nb ingot (Table 3). Among the two alloying additions greater reduction in grain size was observed by the addition of 2.5 wt% Zr, as compared to the addition of 10 wt% W (Table 3). The combined addition of 10 wt% W and 2.5 wt% Zr (Alloy 3) has resulted in much finer grain size (3.6 mm x 0.8 mm) as compared to the alloys containing either 10 wt% W (20 mm × 3.8 mm (Alloy 1) or 2.5 wt% Zr (9.2 mm × 2.5 mm) (Alloy 2). It has been reported that the solute content has significant effects on grain refinement of engineering alloys [15–19]. For effective refinement, not only do the grain refining particles

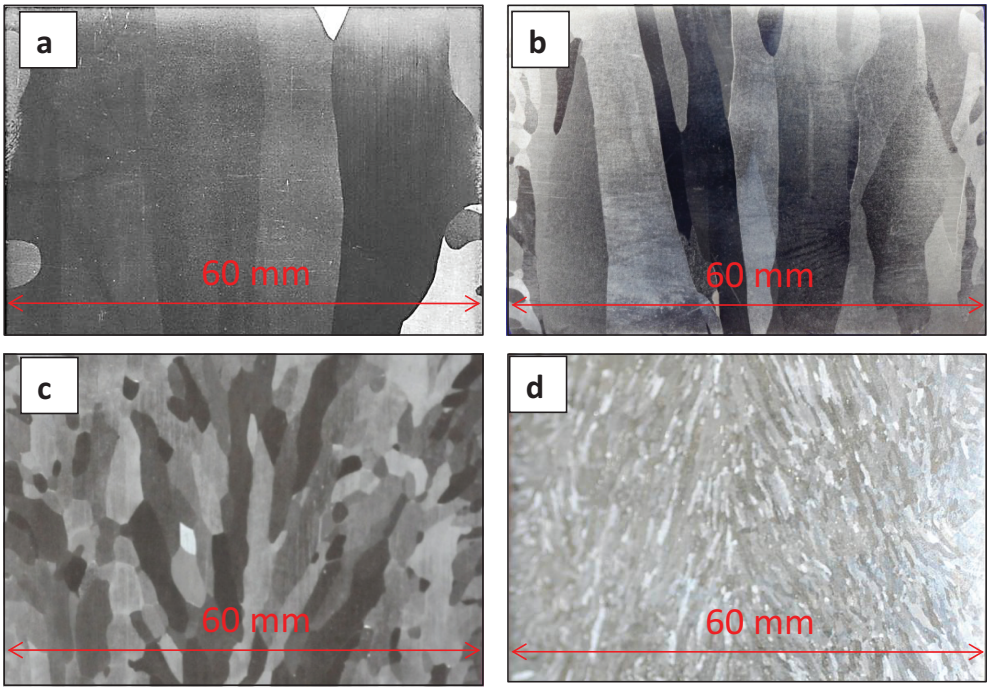

Figure 4: Longitudinal macrostructure of EB drip melted (a) Nb, (b) Nb-10 W, (c) Nb-2.5 Zr and (d) Nb-10 W-2.5 Zr ingots.

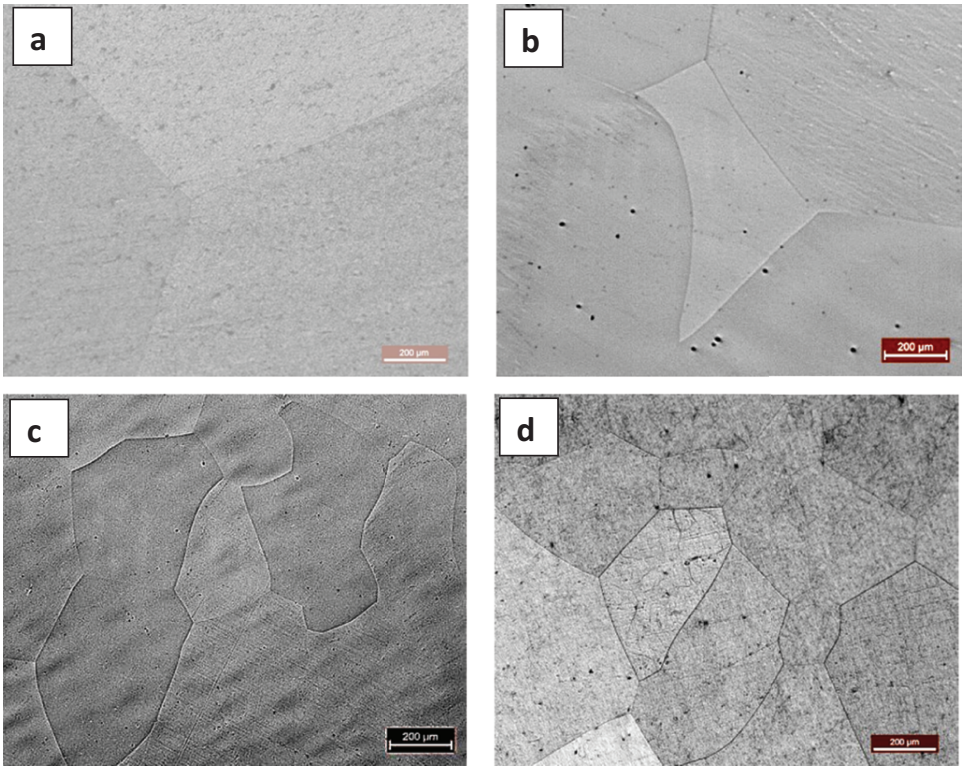

Figure 5: Optical microstructure in transverse direction of EB drip melted (a) Nb, (b) Nb–10 W, (c) Nb–2.5 Zr and (d) Nb–10 W–2.5 Zr ingots.

Table 3: Grain size of EB drip melted ingots.

Alloy	Alloy compositions	Grain size: length (mm) × width (mm)
	Nb	32.4 × 5.6
Alloy 1	Nb–10 W	20 × 3.8
Alloy 2	Nb–2.5 Zr	9.2 × 2.5
Alloy 3	Nb–10 W–2.5 Zr	3.6 x 0.8

themselves need to be potent for heterogeneous nucleation, but some solute segregation is also required to enhance the efficiency of the particles by restricting growth of the solid, either at a columnar growth front competing with equiaxed solidification or from particles where nucleation has already occurred [20–22]. A factor called 'growth restriction factor', $m.C_0.(k-1)$ where m is the slope of the liquidus, C_0 the solute content and k the partition ratio, was proposed by Easton and St. John to compare grain refining potency of various solutes [15]. Recently Man et al. have investigated the effect of solute on grain initiation in an isothermal melt, and developed an analytical model to account for the effect of solute elements on grain size [23]. Their study revealed that the solute elements in the liquid ahead of the growing crystals reduce the growth velocity of the nucleated crystals and increase the maximum undercooling achievable before recoalescence. This allows more particles to be active in nucleation and, consequently, increases the number density of active particles, giving rise to a finer grain size.

In the present work, no inoculants were deliberately added. However, since W and Zr readily form oxides, nitrides and carbides, it is possible that such particles might be present, although in smaller quantities, because of EB refining of the melt with respect to interstitials. Further, the growth restriction factors with respect to W and Zr as solutes in Nb were estimated based on the relevant phase diagrams [24, 25] (Table 4) and found to be 1424 for Zr and 6.3 for W. Based on the comparison, Zr is clearly much more potent solute than W with respect to growth restriction as a mechanism of grain refinement. This might explain the observation of finer grain size in Nb–2.5 wt% Zr compared to Nb–10 wt% W alloy.

Table 4: Growth restriction factors for W and Zr in Nb [14, and ref for phase diagram].

Element	m (°C/wt%)	C_0 (wt%)	k	Growth restriction factor = $m.C_0.k$
W	6.3	10	1.1	6.3
Zr	890	2.5	0.36	1424

X-ray diffraction patterns of Nb and Nb–10 wt% W, Nb–2.5 wt% Zr and Nb–10 wt% W–2.5 wt% Zr alloys are shown in Figure 6. The X-ray diffraction patterns of all the four alloy ingots indicate the presence of single phase with bcc structure. Lattice parameters have

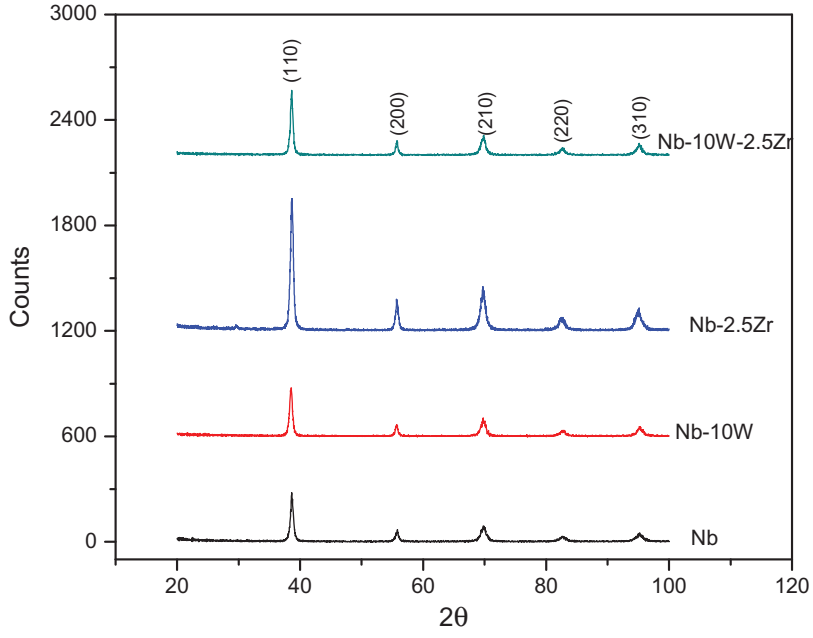

Figure 6: X-ray diffraction pattern for EB drip melted (a) Nb, (b) Nb–10 W, (c) Nb–2.5 Zr and (d) Nb–10 W–2.5 Zr ingots.

been calculated using Bragg's law $\lambda = 2d \sin\theta$ and $d = a/(h2 + k2 + l2)1/2$ (cubic system) for all four alloys corresponding to all of the peaks and tabulated in Table 5. Lattice parameters corresponding to higher angle peaks are selected for more accuracy for all the alloys. W, having the smaller atomic size ($a_{W/}a_{Nb=}$ 0.9569) [26] decreases the lattice parameter of Nb from 3.2992 to 3.2946 while Zr having larger atomic size ($a_{Zr/}$ $a_{Nb=}$ 1.09) [26] increases lattice parameter of Nb from 3.2992 to 3.3078 Å. The combined addition of W and Zr has resulted in a marginal reduction of the lattice parameter of Nb from 3.2992 to 3.2961 Å.

The results of room temperature hardness and tensile properties of EB cast alloy are shown in Table 6. Each hardness data point reported here represents an average of five measurements. Each tensile data point reported represents an average of three tests. Addition of 10 wt% W and 2.5 % wt% Zr has resulted in significant increase in hardness and room temperature tensile strength. It was found that effect of 10 wt% W is more prominent than 2.5 wt% Zr in improving hardness and room temperature tensile strength of Nb. However, when considered on 'per wt%' basis, zirconium is more potent strengthener compared to tungsten (Table 6). It has also been observed that the cumulative effect of 10 wt% W and 2.5 wt% Zr on improvement in strength is more than their individual effects. Both W and Zr have equal effect in bringing down the total elongation before fracture for Nb while their cumulative effect in decreasing the ductility of Nb is more pronounced.

As mentioned in the introduction, Nb-based alloys can be strengthened by a variety of methods such as (a) cold working, (b) solid solution strengthening, and (c) second phase particle strengthening. Apart from these mechanisms, grain boundary strengthening is also to be considered. Solid solution strengthening is generally attributed to (a) atom-size mismatch between

Table 5: Lattice parameter calculations for alloys.

Alloy Composition	d value [Å]	Plane (hkl)	I/Io (Obs.)	I/Io (Ref.)	Cell parameter (Calc.)[Å]	Phases (s) (Ref.) [Å]	Phase	JCPDS card No.
Nb	2.32888	110	100	999	3.2934	3.3	Nb	89–5291
	1.64788	200	20.42	138	3.2958	3.3		
	1.34587	211	26.76	234	3.2994	3.3		
	1.16649	220	8.8	63	3.2992	3.3		
Nb–10 W	2.33007	110	100	999	3.2952	3.3	Nb-W	89–5291
	1.65029	200	22.3	138	3.3006	3.3		
	1.34527	211	31.64	234	3.2952	3.3		
	1.16483	220	4.35	63	3.2946	3.3		
Nb–2.5 Zr	2.33123	110	100	999	3.2969	3.3	Nb-Zr	89–5291
	1.64904	200	22.13	138	3.2981	3.3		
	1.34713	211	28.52	234	3.2998	3.3		
	1.16948	220	7.96	63	3.3078	3.3		
Nb–10 W–2.5 Zr	2.32762	110	100	999	3.2918	3.3	Nb-W-Zr	89–5291
	1.64663	200	20.54	138	3.2933	3.3		
	1.34631	211	28.24	234	3.2978	3.3		
	1.16535	220	5.33	63	3.2961	3.3		

Table 6: Room temperature tensile properties.

Alloy	Material	Hardness (measured) (Hv)	Tensile properties (measured)			Calculated increase in the properties per wt% of the element		
			UTS (MPa)	YS (MPa)	El (%)	Hardness (Hv)	UTS (MPa)	YS (MPa)
	Nb	80	151	125	37	–	–	–
Alloy 1	Nb–10 W	150	298	245	25	7	14.7	12
Alloy 2	Nb–2.5 Zr	115	218	182	27	14	26.8	22.5
Alloy 3	Nb–10 W–2.5 Zr	190	473	423	20	–	–	–

solvent and solute elements and (b) difference in the elastic moduli between the solvent and solute atoms. In the present case, there is about 5 % mismatch between the lattice parameters of Nb and W and, moreover, W has a much higher modulus of elasticity as compared to Nb ($E_W/E_{Nb} = 4.5$) [27]; hence solid solution strengthening by W is to be expected. In addition, grain refinement is observed in Nb-W alloy, which contributes to further strengthening (Table 3). It may also be noted that Nb-W is an isomorphous system [28], which allows higher W to be retained in solid solution at room temperature thus increasing total solid solution strengthening.

Likewise, increase in tensile strength of Nb due to the addition of Zr may be partly attributed to solid solution strengthening due to the 9 % atom-size mismatch between solvent and solute elements ($a_{Zr}/a_{Nb} = 1.09$). However, unlike the case of Nb-W, no modulus strengthening is to be expected from Zr in solution, as the elastic moduli of Zr and Nb are the same [29]. It is interesting to note that, in spite of Zr having no room temperature solubility in Nb, no Zr particles were seen in the microstructure at the optical microscopy level. This could be because of low solvus temperature for Nb-2.5 Zr (~350°C) [30] due to which significant precipitation of zirconium particles is not expected to occur during cooling after solidification or after homogenization treatment. As in the case of Nb-W, grain boundary strengthening is to be expected in Nb-2.5 wt% Zr alloy since grain refinement is observed. Over and above solid solution strengthening and grain boundary strengthening, dispersion strengthening may also occur in Nb-Zr alloys, because of the strong affinity between Zr and the interstitial elements C, O and N which may form fine coherent dispersoids. However, it may be mentioned that no evidence of dispersoids could be established in the present work at optical and SEM levels, and detailed transmission electron microscopy may be needed to verify their existence. Taking into consideration above arguments, the increase in strength due to combined addition of 10 wt% W and 2.5 wt% Zr may be attributed to a combination of solid solution strengthening and grain boundary strengthening, with dispersion strengthening as a possibility. A quantitative treatment of the individual contributions of various strengthening mechanisms is beyond the scope of the present study.

The fractographs of the fracture surfaces of the tensile test specimens of the alloy ingots are shown in Figures 7 and 8. It can be seen from the fractrographs that Nb, Nb–10 W and Nb–2.5 Zr alloys failed largely by ductile mode, as fracture surfaces exhibit essentially dimple features (Figure 7). On the other hand, tensile samples of Nb–10 W–2.5 Zr alloy tested at room temperature failed by quasi cleavage mode with some ductile dimpling (Figure 8).

Summary and conclusions

The individual and combined effects of 10 wt% W and 2.5 wt% Zr additions on macrostructure, microstructure and mechanical properties of Nb have been investigated. The following is the summary of the findings.

1. EB drip melted Nb, Nb–10 W, Nb–2.5 Zr and Nb–10 W–2.5 Zr ingots exhibit rippled surface finish which is characteristic of semi-continuous casting processes. All the three alloys exhibit single phase microstructure at optical microscope level and have bcc crystal structure.
2. 10 wt% W marginally decreases, while 2.5 wt% Zr addition marginally increases the lattice parameter of Nb. The combined addition of 10 wt% W and 2.5 wt% Zr decreases the lattice parameter of Nb but to even a lesser extent than individual addition of W, possibly due to the opposing effect of Zr on lattice parameter of Nb.
3. Individual additions of either 10 wt% W or 2.5 wt% Zr resulted in grain refinement of Nb during EB casting. Among the two elemental additions, Zr is more potent as a grain refiner than W, which is explained based on the ‘growth restriction factor’. The greatest grain refinement occurs when the above quantities of W and Zr are added together.
4. Addition of 10 wt% W and 2.5 wt% Zr to Nb results in significant increase in hardness and room temperature tensile strength. On per wt% addition basis, Zr is more effective than W in improving hardness and room temperature strength of Nb. It has also been observed that the cumulative effect of W and Zr on improvement in strength is more than the algebraic sum of their individual effects.
5. Strengthening of Nb by W and Zr is explained based on solid solution strengthening and grain boundary strengthening. Although Zr has no solubility in Nb at room temperature, it appears to be retained in solid solution under prevailing processing conditions, possibly due to low diffusivity of Zr below the solvus temperatures.

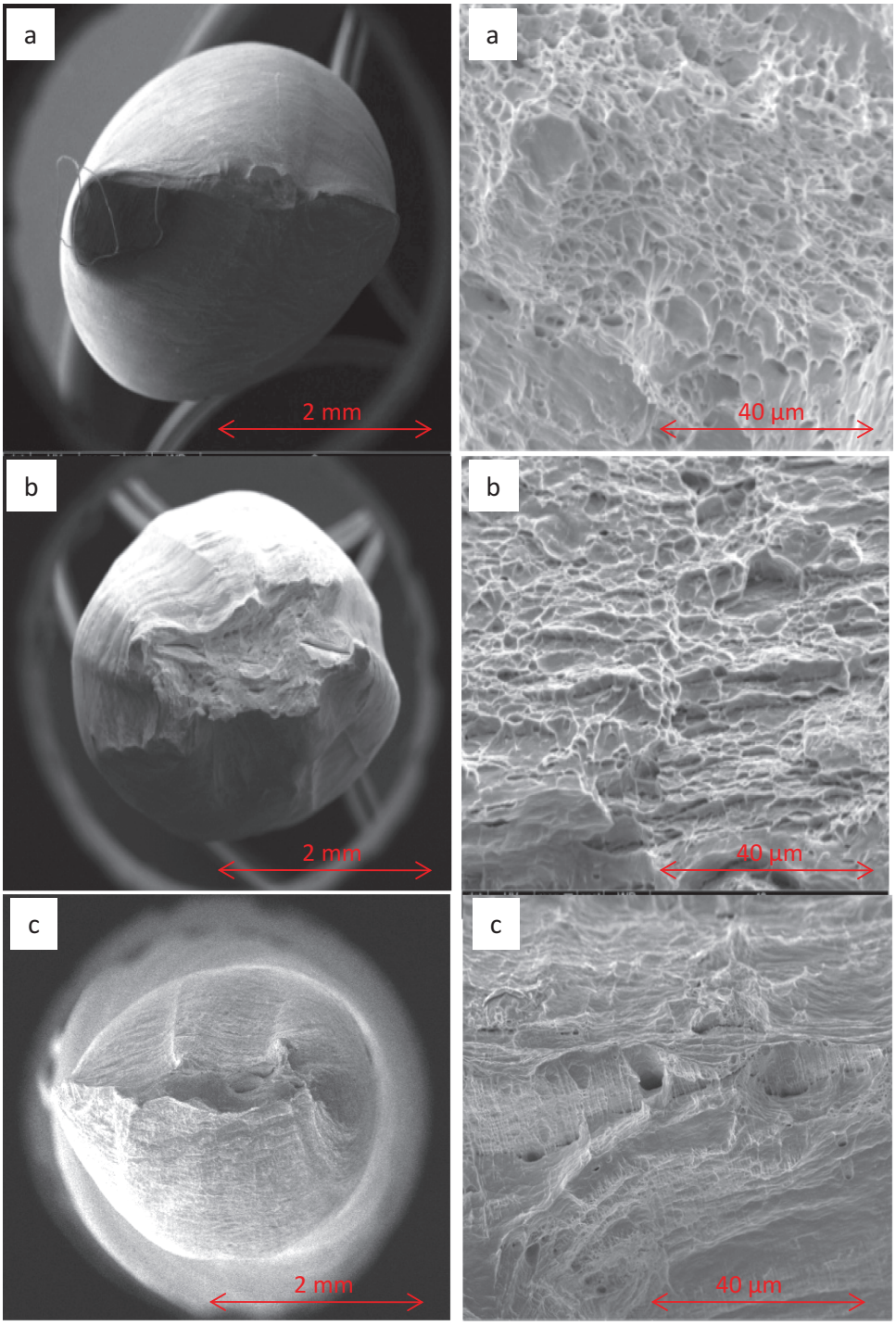

Figure 7: SEM photographs showing the room temperature tensile fracture of EB drip melted (a) Nb, (b) Nb–10 W, and (c) Nb–2.5 Zr ingots.

Acknowledgements: The authors are sincerely thankful to DRDO for financial assistance through project DMR-295 for carrying out these studies. The authors would like to express sincere gratitude to Dr. Samir V. Kamat, Director DMRL for his constant encouragement to carry out the present work. Authors also would like to thank the staff members of ERG, MJG, MBG, MWG, EMG, ACG and SFAG for their help in experimentation.

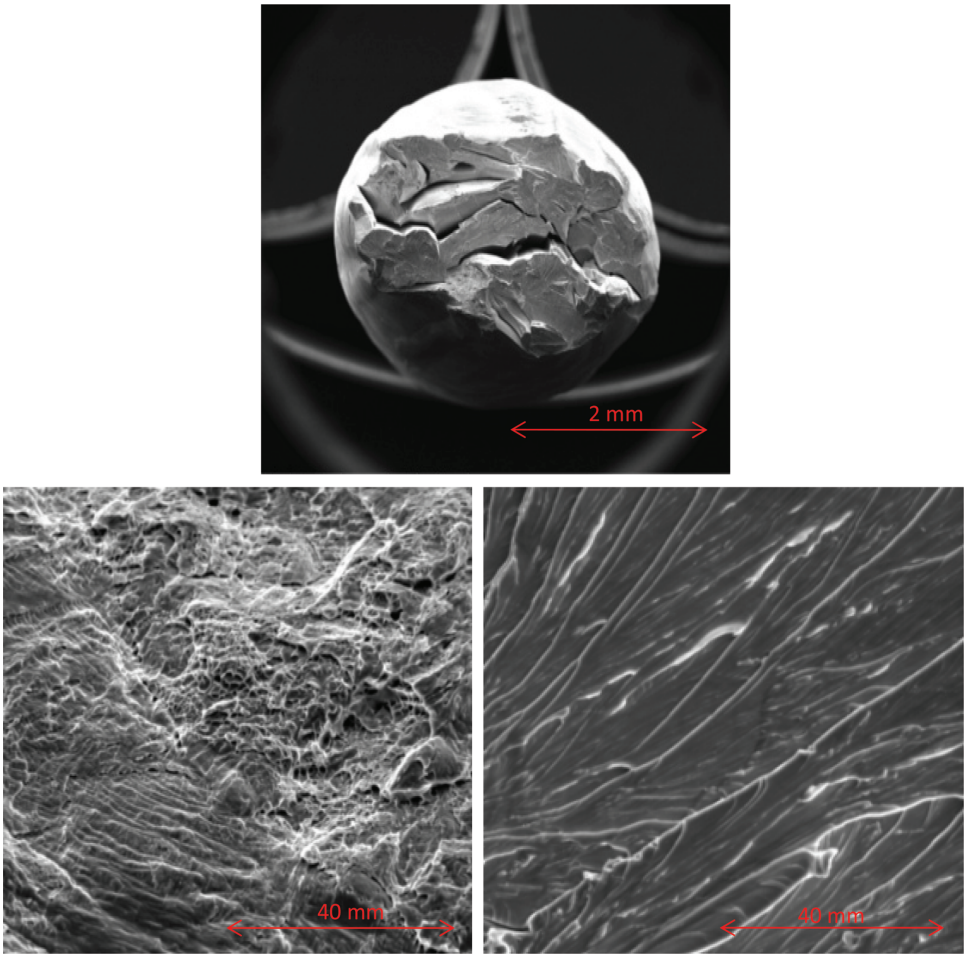

Figure 8: SEM photographs showing the room temperature tensile fracture of EB drip melted. Nb–10 W–2.5 Zr.

References

[1] J.J. Stephens, Jom, 42(8) (1990) 22–23.
[2] J. Wittenauer, Jom, 42(8) (1990) 7–10.
[3] B.A. Wilcox, Chapter 1 in Refractory Metal Alloys Metallurgy and Technology edited by I. Machlin, R.T. Begley and E.D. Weisert, Plenum Press, New York (1968), pp. 1–39.
[4] H. Chen, A. Kauffmann, B. Gorr, D. Schliephake, C. Seemüller, J. N. Wagner, H.-J. Christ and M. Heilmaier, J. Alloys Compd., 661 (2016) 206–215.
[5] S. Shi, L. Zhu, H. Zhang and Z. Sun, Mater. Lett., 189 (2017) 310–312.
[6] R.G. Frank, Chapter 7 in Refractory Metal Alloys Metallurgy and Technology edited by I. Machlin, R.T. Begley and E.D. Weisert, Plenum Press, New York (1968), pp. 325–365.
[7] J.A. Cornie, Development of Precipitation Strengthened Columbium Base Alloys, AFML TR–71-51, Air Force Materials Laboratory, Ohio (1971).
[8] T.K. Roche and D.L. Graham, Development of Oxidation Resistant High Strength Columbium Alloys, AFML TR–69-344, Air Force Materials Laboratory, Ohio (1970).
[9] J. Eckert, Chapter 7 in Handbook of Extractive Metallurgy edited by F. Habashi, Wiley-Vch, Canada (1997), pp. 1403–1416.
[10] C.C. Wojcik, Adv. Mater. Process., 154(6) (1998) 27–30.
[11] O.N.O. Katsutoshi and K.Y. Hawn, ISIJ Int., 32(5) (1992) 650–655.
[12] A. Choudhary and E. Hengsberger, ISIJ Int., 32(5) (1992) 673–681.
[13] M.S. Shishir, Y. Satish Reddy, V.V. Satya Prasad, R.G. Baligidad, K.V. Mirji and A.A. Gokhale, Feasibility Study for Preparation of Cb-752 Alloy through EB Melting, DRDO-DMRL-ERG-106, Defence Metallurgical Research Laboratory, Hyderabad (2015).
[14] P. Alex, J.K. Kumhar, R.C. Hubli, J.K. Chakravartty, K.V. Mirji and N. Saibaba, Development of Nb-1Zr-0.1C Alloy by Direct Aluminothermic Reduction of Oxides and Electron Beam Melting, BARC-I-008, Bhabha Atomic Research Centre, Mumbai (2014).
[15] M. Easton and D. St. John, Metall. Mater. Trans., A, 30 (1999) 1613–1623.
[16] D.H. St. John, M. Qian, M.A. Easton, P. Cao and Z. Hildebrand, Metall. Mater. Trans., A, 36 (2005) 1669–1679.
[17] D.G. McCartney, Int. Mater. Rev., 34 (1989) 247–260.
[18] B.S. Murty, S.A. Kori and M. Chakraborty, Int. Mater. Rev., 47 (2002) 3–29.
[19] T.V. Atamanenko, D.G. Eskin, L. Zhang and L. Katgerman, Metall. Mater. Trans., A, 41 (2010) 2056–2066.
[20] A.M. Bunn, P. Schumacher, M.A. Kearns, C.B. Boothroyd and A.L. Greer, Mater. Sci. Technol., 15 (1999) 1115–1123.

[21] J.D. Hunt, Mater. Sci. Eng., 65 (1984) 75–83.
[22] M. Gaumann, R. Trivedi and W. Kurz, Mater. Sci. Eng., A, 226–228 (1997) 763–769.
[23] H. Men and Z. Fan, Acta Mater., 59 (2011) 2704–2712.
[24] Nb-W phase diagram calculated by MTDATA – Phase Diagram Software from the National Physical Laboratory, United Kingdom. http://resource.npl.co.uk/mtdata/phdiagrams/nbw.htm
[25] Nb-Zr phase diagram calculated by MTDATA – Phase Diagram Software from the National Physical Laboratory, United Kingdom http://resource.npl.co.uk/mtdata/phdiagrams/nbzr.htm
[26] W. Hume Rothery and G.V. Raynor, The Structure of Metals and Alloys, Institute of Metals, London (1954).
[27] F.H. Featherston and J.R. Neighbours, Phys. Rev., 130 (1963) 1324–1333.
[28] ASM Handbook: Alloy Phase Diagrams edited by H. Okamoto, M.E. Schlesinger and E.M. Mueller, ASM International, Materials Park, Ohio (1992), pp. 2304–2308.
[29] G.L. Miller, Metallurgy of the Rarer Metals: Zirconium, Butterworths, London (1957).
[30] ASM Handbook: Binary Alloy Phase Diagrams edited by T.B. Massalski, H. Okamoto, P.R. Subramanian and L. Kacprzak, Materials Park, Ohio (1986), pp. 1710–1711.